

Twisted Vortex State

V. B. Eltsov,^{1,2} A. P. Finne,¹ R. Hänninen,³ J. Kopu,¹ M. Krusius,¹ M. Tsubota,³ and E. V. Thuneberg⁴

¹Low Temperature Laboratory, Helsinki University of Technology, P.O. Box 2200, 02015 HUT, Finland

²Kapitza Institute for Physical Problems, Kosygina 2, 119334 Moscow, Russia

³Department of Physics, Osaka City University, Sugimoto 3-3-138, Sumiyoshi-ku, Osaka 558-8585, Japan

⁴Department of Physical Sciences, P.O. Box 3000, 90014, University of Oulu, Finland

(Received 28 February 2006; published 1 June 2006)

We study a twisted vortex bundle where quantized vortices form helices circling around the axis of the bundle in a “force-free” configuration. Such a state is created by injecting vortices into a rotating vortex-free superfluid. Using continuum theory we determine the structure and the relaxation of the twisted state. This is confirmed by numerical calculations. We also present experimental evidence of the twisted vortex state in superfluid ³He-B.

DOI: 10.1103/PhysRevLett.96.215302

PACS numbers: 67.57.Fg, 47.32.-y, 67.40.Vs

The equilibrium state of a superfluid under rotation consists of an array of quantized vortices, which are parallel to the rotation axis. Similarly, the equilibrium state of a type II superconductor in a magnetic field consists of an array of flux lines parallel to the field. Here we consider twisted vortex states where the vortices have a helical configuration circling a common axis. An example would be a vortex bundle deformed under torsion. One type of twisted vortex state appears in a superconducting current-carrying wire in parallel external magnetic field [1–3]. The current induces a circular magnetic field, which makes the field lines helical, and in order to be *force free*, the flux lines take the same conformation. Here we concentrate on a new type of twisted state, which can occur even when the driving field is a constant. Only this second type can appear in charge-neutral superfluids, where the rotation is not affected by currents.

In this Letter we demonstrate that the twisted vortex state appears spontaneously when vortex lines expand into vortex-free rotating superfluid. We present analytical results for the twisted state using the continuum theory of vorticity. In particular, we state the equilibrium force-free conditions for a uniformly twisted state, and find the equations governing the relaxation of a nonuniform twist. We present numerical simulations for both the generation and the relaxation of the twist. We discuss the stability of the twisted state, which is limited by the *helical instability* [4,5]. The results are valid in superfluids and also in superconductors in the limit of large penetration depth and no pinning. Finally, we present experiments that show evidence of the twisted vortex state in superfluid ³He-B.

Generation.—We study superfluid in a long cylinder that rotates around its axis. We assume that initially the system is in metastable state, where no vortex lines are present. Then a bunch of vortex loops is created at some location. They start to expand along the cylinder. A snapshot from our numerical simulation of such propagating vortices is shown in Fig. 1. Two striking observations can be made. First, the vortices form a front, where the ends of the lines bend to the sidewall. Second, the growing vortex bundle

behind the front is twisted, because the front rotates at a different speed than vertical vortex sections. The existence of the front is deduced from simulation and experiment. Here we concentrate on the twisted state behind the front.

The equilibrium state of the superfluid consists of an array of rectilinear vortex lines at areal density $n_v = 2\Omega/\kappa$, where Ω is the angular velocity and κ the circulation quantum [6]. The superfluid velocity \mathbf{v}_s at the location

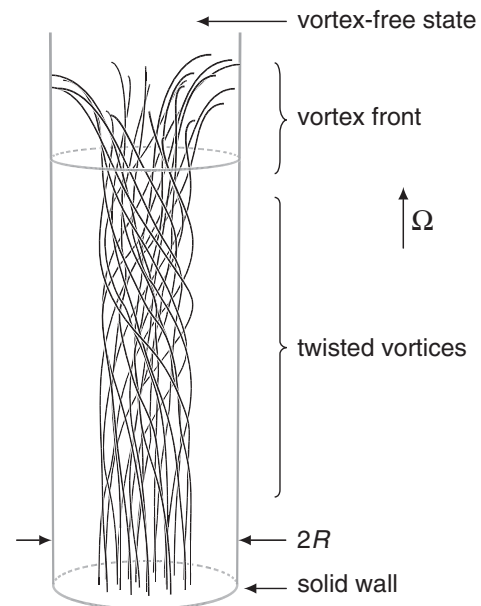


FIG. 1. The formation of twisted vortex state. The vortices have their propagating ends bent to the sidewall of the rotating cylinder. As they expand upwards into the vortex-free state, the ends of the vortex lines rotate around the cylinder axis. The twist is nonuniform because boundary conditions allow it to unwind at the bottom solid wall. The figure gives a snapshot (at time $t = 25 \Omega^{-1}$) of a numerical simulation of 23 vortices initially generated near the bottom end ($t = 0$). The parameters are $2\pi\Omega R^2/\kappa = 86$, $\alpha = 0.18$, and $\alpha' = 0.16$ [15], and $R/a = 3 \times 10^5$, which corresponds to $T = 0.4T_c$ in ³He-B at 29 bar pressure. For time evolution see Ref. [16].

of each vortex is precisely equal to the normal fluid velocity $\mathbf{v}_n = \boldsymbol{\Omega} \times \mathbf{r}$, so that the array rotates rigidly together with the cylindrical container. In contrast, the superfluid velocity vanishes in the vortex-free state, $\mathbf{v}_s \equiv 0$. All velocities are given in the laboratory frame.

Next we determine the rotation of the vortex ends on the sidewall. For simplicity we consider zero temperature, where the velocity of a vortex line \mathbf{v}_L is equal to the local superfluid velocity. The average superfluid velocity in the vortex front is the average of \mathbf{v}_s between the vortex state and the vortex-free state. This gives that the average angular velocity of the front is half of the container velocity, $\langle \dot{\phi} \rangle = \Omega/2$. Thus the vortex front lags behind the vortex array which gives rise to the twisted vorticity.

It is interesting that the angular velocity of the front can also be determined from alternative arguments. One is based on the Hamiltonian equations $\dot{\phi} = \partial H / \partial L$ and $\dot{L} = -\partial H / \partial \phi$, where L is the component of angular momentum along the cylinder axis z . Shifting the vortex front vertically, the former equation gives $\dot{\phi} = \Delta E / \Delta L$, where ΔE is the energy difference and ΔL the angular momentum difference between the vortex and vortex-free states. Evaluating these using the continuum model of vorticity ($\mathbf{v}_s \approx \boldsymbol{\Omega} \times \mathbf{r}$ in the vortex state) gives the same result as above. This result is also easy to generalize to the case where the vortex number N is smaller than in equilibrium, and the result is

$$\dot{\phi} = \frac{N\kappa}{2\pi} \frac{\ln(R/R_v) + 1/4}{R^2 - R_v^2/2}, \quad (1)$$

where $R_v^2 = N\kappa/2\pi\Omega$. A third argument relies on the Josephson relation, where the rotating vortex ends cause a phase slippage to compensate the chemical potential difference between the two states [7]. The rotation of one vortex in agreement with Eq. (1) has been observed experimentally by Zieve *et al.* in a cylinder with a wire on the axis and zero applied flow [8].

Uniform twist.—We construct a description of the twisted vortex state using the continuum model of vorticity [6,9,10]. We start by considering a twisted state which has translation and circular symmetry. This limits the superfluid velocity to the form

$$\mathbf{v}_s = v_\phi(r)\hat{\phi} + v_z(r)\hat{z}, \quad (2)$$

in cylindrical coordinates (r, ϕ, z) . It is straightforward to calculate the vorticity $\boldsymbol{\omega} = \nabla \times \mathbf{v}_s$. The motion of a vortex (velocity \mathbf{v}_L) is determined by the general equation

$$\mathbf{v}_L = \tilde{\mathbf{v}}_s + \alpha\hat{s} \times (\mathbf{v}_n - \tilde{\mathbf{v}}_s) - \alpha'\hat{s} \times [\hat{s} \times (\mathbf{v}_n - \tilde{\mathbf{v}}_s)]. \quad (3)$$

This includes the mutual friction between the vortex lines and the normal fluid with coefficients α and α' . Here \hat{s} is a unit vector along a vortex line and $\tilde{\mathbf{v}}_s$ is the superfluid velocity at the vortex core. In continuum theory $\hat{s} = \hat{\boldsymbol{\omega}}$ (the unit vector along $\boldsymbol{\omega}$), and $\tilde{\mathbf{v}}_s = \mathbf{v}_s + \nu\nabla \times \hat{\boldsymbol{\omega}}$ differs from the average velocity \mathbf{v}_s by a term caused by the vortex curvature [6]. In our case it is a small correction but is

included for completeness. Here $\nu = (\kappa/4\pi) \ln(b/a)$, b is the vortex spacing, a the core radius. Note that only the component perpendicular to \hat{s} of Eq. (3) is relevant since \mathbf{v}_L parallel to \hat{s} is of no consequence.

We require that vortices do not move radially in the twisted state (2). This gives the condition

$$(\Omega r - v_\phi) \left(\frac{v_\phi}{r} + \frac{dv_\phi}{dr} \right) - v_z \frac{dv_z}{dr} + \frac{\nu}{|\boldsymbol{\omega}|r} \left(\frac{dv_z}{dr} \right)^2 = 0. \quad (4)$$

Moreover, this condition implies that all frictional forces vanish since the twisted vortices rotate uniformly with the cylinder, $\mathbf{v}_L = \boldsymbol{\Omega} \times \mathbf{r}$. The only deviation from solid body rotation on the average is swirling \mathbf{v}_s that everywhere is parallel to the twisted vortices. We conclude that Eqs. (2) and (4) represent a family of stable uniformly twisted states. The wave vector $Q = \omega_\phi / \omega_z r$ of the twist is an arbitrary function of the radial coordinate, $Q(r)$. An explicitly solvable case is obtained by choosing a constant Q and neglecting ν :

$$v_\phi(r) = \frac{(\Omega + Qv_0)r}{1 + Q^2r^2}, \quad v_z(r) = \frac{v_0 - Q\Omega r^2}{1 + Q^2r^2}. \quad (5)$$

An important property of the twisted states is the flow parallel to the axis, $v_z(r)$. Assuming that there is no net flow gives an integral condition for $v_z(r)$. In the case of Eq. (5) this implies $v_0 = (\Omega/Q)[Q^2R^2/\ln(1 + Q^2R^2) - 1]$. The deviation of v_ϕ from Ωr implies that vortices are more compressed in the center and diluted at larger r compared to equilibrium rectilinear vortices.

We note that also the Navier-Stokes equations have a stationary solution for uniform swirling flow, but only under a pressure gradient along z . The twisted state is closely related to the inertia wave in rotating classical fluids. Various forms of twisted vorticity as solutions of the Euler equation have been studied in the literature [11].

Nonuniform twist.—Next we construct equations governing the relaxation of twisted vortices. Now all components (v_r, v_ϕ, v_z) of \mathbf{v}_s are nonzero and functions of r, z , and time t . Here we take into account only first order deviations from the rotating equilibrium state. The dynamical equations can be formed using again Eq. (3) for \mathbf{v}_L , to obtain equations for the radial and azimuthal coordinates of vortices. These together with the continuity equation and $\boldsymbol{\omega} = \nabla \times \mathbf{v}_s$ form a closed set of equations. The same set of equations has been derived previously starting from the dynamical equation for \mathbf{v}_s [4,12]. The essential result is the dispersion relation [4,12]

$$\frac{(\beta^2 + k^2)\sigma}{\Omega} = -i\alpha(\beta^2 + 2k^2\eta_2) \pm i\sqrt{\alpha^2\beta^4 - 4(1 - \alpha')^2k^2(\beta^2 + k^2)\eta_1\eta_2}. \quad (6)$$

The waves giving rise to this dispersion are of the form $v_r = ckJ_1(\beta r) \exp(ikz - i\sigma t)$ and $v_z = ic\beta J_0(\beta r) \times \exp(ikz - i\sigma t)$. J_0 and J_1 are Bessel functions, while

$\eta_1 = 1 + \nu k^2/2\Omega$ and $\eta_2 = 1 + \nu(\beta^2 + k^2)/2\Omega$. The boundary condition $v_r(R) = 0$ leads to $\beta = 3.83/R, 7.01/R, \dots$. We study the case that the square root in Eq. (6) is real. Then the negative sign corresponds to radial motion of vortices (which induces also azimuthal motion). Here we are interested in the positive sign, which corresponds to twisting the vortex state. In this case the frequency σ vanishes for vanishing wave vector k . This is in agreement with our preceding analysis that there is no relaxation of the uniformly twisted state. For a nonuniform twist we have to consider a finite k , but still assume $k \ll R^{-1}$. The dispersion relation (6) then simplifies to $\sigma = -ik^2(2\Omega/\beta^2 + \nu)/d$, where d is another mutual friction coefficient $d = \alpha/[(1 - \alpha')^2 + \alpha^2]$. This limit corresponds to the diffusion equation

$$\frac{\partial f}{\partial t} = D \frac{\partial^2 f}{\partial z^2}, \quad D = \frac{1}{d} \left(\frac{2\Omega}{\beta^2} + \nu \right), \quad (7)$$

with effective diffusion constant D . Here $f(z, t)$ can be either v_r or v_z . We see that the diffusion gets faster towards lower temperatures, where the friction coefficients approach zero.

Simulation.—We have tested the previous theory with numerical calculations. In the initial state we have placed a number of vortices at one end of a rotating cylinder so that they bend from the bottom to the sidewall. The dynamics is determined by calculating $\tilde{\mathbf{v}}_s$ in Eq. (3) from the Biot-Savart integral [13]. We assume $\mathbf{v}_n = \boldsymbol{\Omega} \times \mathbf{r}$. An illustrative case with a small number of vortices is shown in Fig. 1. Another case with more vortices is examined in Fig. 2 together with the averaged axial and azimuthal velocity profiles.

The essential features in Fig. 2 are the vortex-free state in the upper part of the cylinder, the propagating vortex front, and the twisted vortex state that is left behind. In the front v_ϕ increases rapidly so that the azimuthal counterflow $v_\phi - \Omega r$ is strongly reduced in absolute value. While the vortex front progresses, the vortex ends rotate at a lower speed than the cylinder. This generates the twisted vortex state. A clear signature of the twist is the axial velocity v_z . It is downwards in the center and upwards in the periphery (corresponding to a left-handed twist, $Q < 0$). At the bottom wall the boundary condition prohibits any axial flow. This implies that the twist vanishes there. We assume that the vortex ends can slide with respect to the bottom wall. Thus the winding generated by the front is unwound at the bottom.

The calculations indicate that the vortex front deviates from any equilibrium configuration and probably cannot be described by simple analytic theory. On the other hand, the relaxing twist seems to obey the diffusion equation (7). The profile of v_z in Fig. 2 can be understood as relaxation towards a steady state where v_z is linear in z .

The twist implies superflow parallel to the vortex lines. In such a case it is expected that individual vortices can become unstable against helical distortion. A calculation in

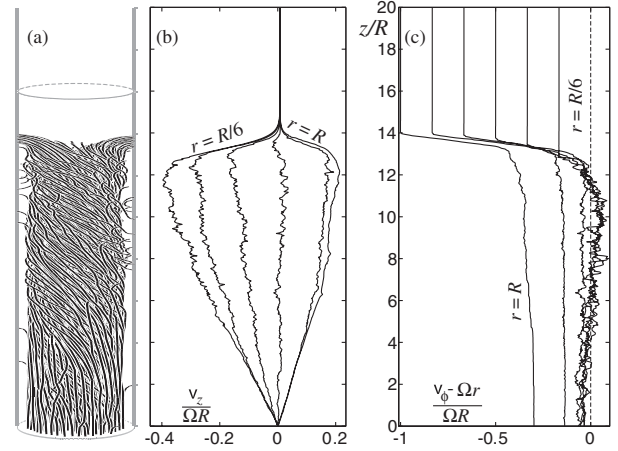


FIG. 2. A snapshot of the numerically calculated vortex state expanding along z : (a) vortex configuration, (b) axial v_z , and (c) azimuthal v_ϕ components of the superflow velocity. The velocities, plotted as functions of z , are averaged over the azimuthal angle and are shown at radii $r = nR/6$ with integer n . Note that $v_\phi - \Omega r$ changes sign in (c) close to the center of the bundle, as predicted by Eq. (5). The simulation was started with 203 vortices and the picture was taken after a time interval of $60 \Omega^{-1}$. The parameters are the same as in Fig. 1 except $2\pi\Omega R^2/\kappa = 214$, $R/a = 1.5 \times 10^5$. For clarity, r and z coordinates have different scales in (a).

Ref. [4] predicts this *helical instability* to take place for rectilinear vortices when the velocity of the parallel flow reaches $v_z = 2\sqrt{2\Omega\nu}$. The simulations indicate that the maximum axial velocity v_z (see Fig. 2) remains smaller than this limit. It appears that if any tighter twist is created in the front, it is immediately relaxed by instabilities and subsequent vortex reconnections. Note that the same helical instability is responsible for flux flow in the force-free configurations in superconductors [2,5].

Experiment.—We now turn to the evidence for the twisted vortex state from NMR measurements on a rotating sample of $^3\text{He-B}$. The experimental details have been described in Ref. [14]. What is essential is that the NMR absorption is measured at two symmetric locations near the ends of the long sample cylinder. A measuring run is shown in Fig. 3. The vortices are injected in the middle of the cylinder at time $t = 0$. Then the NMR line shapes change in both locations simultaneously from the initial vortex-free form ($N = 0$ spectrum in the inset of Fig. 3) to that of the final equilibrium vortex state ($N = N_{\text{eq}}$ spectrum). During the transition the absorption is first shifted from a “counterflow” peak to an overshoot in the “Larmor region” and later redistributed more evenly over the entire spectrum. By tuning one spectrometer on the counterflow peak and the other on the peak in the Larmor region, the timing of the two peaks is resolved in the main panel. We see that after a flight time of 22 s, the vortex fronts reach the spectrometers. The spectrometer tuned to the counterflow peak sees a rapid drop in absorption. The other spectrometer tuned to the Larmor peak records first a rapid

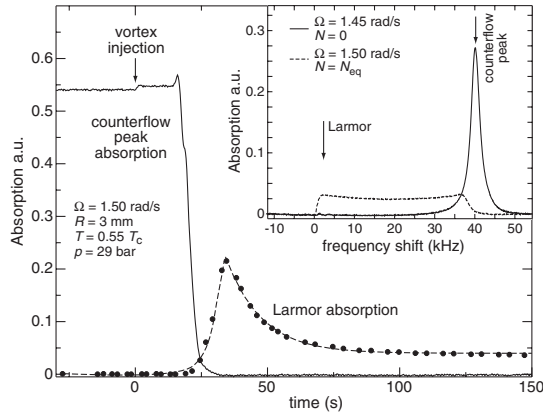


FIG. 3. NMR absorption signals as a function of time after injection of vortices at $t = 0$. The two NMR absorption records in the *main panel* show the reduction in the counterflow peak and the overshoot in the Larmor region. The former is interpreted as the arrival of the vortex front and the rapid increase in v_ϕ . The latter arises from the axial flow velocity v_z , caused by twisted vortices, and the subsequent slow relaxation towards the equilibrium state. The *inset* shows the NMR line shapes in the initial vortex-free state $N = 0$ and the final equilibrium vortex state $N = N_{eq}$. The spectra are measured at constant temperature and have the same integrated absorption.

increase, followed by a slow exponential relaxation with a time constant of 14 s towards the final level of the equilibrium vortex state.

The quantitative interpretation of the two signals requires detailed analysis of order parameter textures in $^3\text{He-B}$ with curved vortices and will be presented elsewhere. Very simply, though, a large counterflow peak comes from counterflow $\mathbf{v}_n - \mathbf{v}_s$ that is perpendicular to the rotation axis z (when the static magnetic field is along z). Conversely, large absorption near the Larmor frequency comes from counterflow parallel to z . Because z is a symmetry direction, there is always some absorption near the Larmor frequency, but it is modest under normal circumstances, where no axial flow is present ($N = N_{eq}$ spectrum in Fig. 3).

The transient absorption traces in Fig. 3 can now be understood as a measurement of the vortex state in Fig. 2 at a fixed detector location z_{det} . The arrival of the vortex front at z_{det} causes an abrupt reduction in the counterflow peak as $|\mathbf{v}_\phi - \Omega r|$ is reduced. Simultaneously v_z is increasing which is seen as a rise in the Larmor absorption. The subsequent decrease of v_z after the passage of the front is seen as relaxation of the Larmor absorption towards the equilibrium vortex state.

The time constant for the decay of the Larmor absorption is plotted in Fig. 4 as a function of temperature together with the slowest mode from the diffusion Eq. (7). We note that the theoretical eigenvalue is in order of magnitude agreement with the measurements. It is especially noteworthy that relaxation gets faster with de-

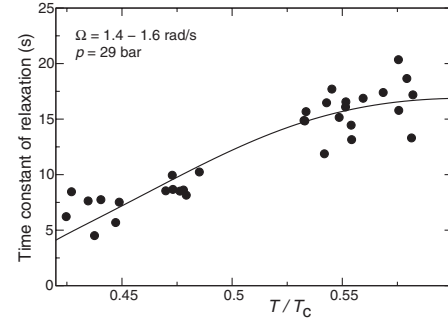


FIG. 4. The time constant for the decay of the Larmor absorption (data points) compared to the decay of the twisted state according to the slowest mode of Eqs. (6) and (7) (line). The line has $k = \pi/\ell$ as fitting parameter giving $\ell = 18$ mm. For comparison, the half length of the cylinder is 55 mm and the detector coil is placed between 5 and 15 mm distance from the end plate [14].

creasing temperature. This may at first seem surprising since the relaxation is usually associated with friction, which decreases with decreasing temperature. Our simulations, which are time consuming at the experimental parameter values, yield a time constant which is larger but within a factor of 3 from the experimental value.

In conclusion, in a rotating superfluid a front followed by a twisted vortex bundle is the preferred configuration of vortex expansion, rather than a turbulent tangle, when the induced supercurrents remain below the helical instability limit. It appears feasible that a similar state can be generated in a superconductor in the superclean limit.

We thank N. Kopnin, E. Sonin, and G. Volovik for useful comments.

-
- [1] D. G. Walmsley, *J. Phys. F* **2**, 510 (1972).
 - [2] E. H. Brandt, *Rep. Prog. Phys.* **58**, 1465 (1995).
 - [3] R. D. Kamien, *Phys. Rev. B* **58**, 8218 (1998).
 - [4] W. I. Glaberson, W. W. Johnson, and R. M. Ostermeier, *Phys. Rev. Lett.* **33**, 1197 (1974).
 - [5] J. R. Clem, *Phys. Rev. Lett.* **38**, 1425 (1977).
 - [6] H. E. Hall, *Adv. Phys.* **9**, 89 (1960).
 - [7] T. Sh. Misirpashaev and G. E. Volovik, *Pis'ma Zh. Eksp. Teor. Fiz.* **56**, 40 (1992) [*JETP Lett.* **56**, 41 (1992)].
 - [8] R. J. Zieve *et al.*, *Phys. Rev. Lett.* **68**, 1327 (1992).
 - [9] I. L. Bekarevich and I. M. Khalatnikov, *Zh. Eksp. Teor. Fiz.* **40**, 920 (1961) [*Sov. Phys. JETP* **13**, 643 (1961)].
 - [10] E. B. Sonin, *Rev. Mod. Phys.* **59**, 87 (1987).
 - [11] G. K. Batchelor, *An Introduction to Fluid Dynamics* (Cambridge University Press, Cambridge, England, 1988); V. L. Okulov, *J. Fluid Mech.* **521**, 319 (2004).
 - [12] K. L. Henderson and C. F. Barenghi, *Europhys. Lett.* **67**, 56 (2004).
 - [13] R. Hänninen *et al.*, *J. Low Temp. Phys.* **138**, 589 (2005).
 - [14] A. P. Finne *et al.*, *J. Low Temp. Phys.* **136**, 249 (2004).
 - [15] T. D. C. Bevan *et al.*, *J. Low Temp. Phys.* **109**, 423 (1997).
 - [16] See <http://ltd.tkk.fi/research/theory/twist.html>.